Asymmetric co-substrate usage at a metabolic branch point can drive overflow metabolism

Robert West[1], Sonal[2], Tailise D.S.G. Rodrigues[1,*], Wenying Shou[2], and Orkun S. Soyer[1,†]

[1]School of Life Sciences, University of Warwick, UK
[2]Genetics, Evolution and Environment, University College London, UK
[†]Corresponding author, *O.Soyer@warwick.ac.uk*
[*]Current address: Living Systems Institute, University of Exeter

1 Abstract

Metabolic behaviours of cells, such as metabolic overflow, involve regulation of metabolic fluxes across different pathways. Two well-established concepts in flux regulation are transcriptional regulation, involving changes in enzyme levels through gene regulation, and allosteric regulation, involving changes in enzyme catalytic activities through metabolite binding. Here, we describe an additional mechanism arising through co-substrate usage around metabolic branch points. Using models of different branch-point motifs, we find that asymmetric usage of a given co-substrate by reactions at and around a branch point induces flux switching at that branch point as influx increases. This provides cells with an inherent 'self-regulation' embedded in the architecture of metabolic pathways. We then develop a specific model of the yeast pyruvate branch point involving NADH usage. Using this model, we show that co-substrate based flux switching can explain experimental data on yeast metabolic overflow at high glucose influx, as well as how altering NADH dynamics shifts the initiation point of metabolic overflow. We conclude that asymmetric co-substrate utilisation around branch points provides an inherent regulatory mechanism that could explain observed relations between co-substrate dynamics and metabolic behaviours. Additionally, the presented theory and its extensions will provide a model-based approach to manipulating co-substrate dynamics for metabolic engineering.

2 Introduction

Overflow metabolism, also known as aerobic glycolysis, 'Warburg' or 'Crabtree' effect, is a broadly observed cellular phenomenon, seen in mammalian cells, yeast, and bacteria [4, 12, 50, 34, 6]. It involves an increased flux into fermentation products, such as lactate, ethanol, and acetate, with increasing glucose consumption rates, despite aerobic conditions and continued respiration [12, 46]. Since respiration produces more ATP per glucose compared to fermentation, and since cells achieve a higher growth rate under respiro-fermentation [45, 6, 4], metabolic overflow is seen as cells trading-off efficiency in energy harvesting for growth rate [46, 35].

Despite this fundamental relevance and seemingly universal presence across species, the underpinning causes of overflow metabolism are still unclear. At an abstract level, overflow metabolism is explained as arising from cellular constraints [26]. At a mechanistic level, however, the exact cause of such a constraint is unclear. For instance, several modelling studies proposed that the protein synthesis can become a constraint under fast growth conditions, and that the switching to fermentation would result due to the lower protein cost of fermentation compared to respiration [4, 29]. This suggestion leads to the hypothesis that metabolic overflow results from cells increasing the levels of fermentation pathway enzymes over those in the respiration

pathways. Proteomics-based measurements, however, are inconclusive on the extent of changes in pathway-specific enzyme levels [28, 33, 15]. In addition, recent experimental studies report contrasting results on protein efficiency of fermentation vs. respiration [39, 22]. Finally, flux responses to perturbations, including overflow response, can happen within seconds or few minutes [34, 49] and, in general, cannot be explained solely by changes in enzyme expression levels [11, 15, 49, 16]. These findings show that protein-based constraints, on their own, cannot explain overflow metabolism [39, 11].

Within central metabolism, metabolic overflow specifically relates to a branch point involving pyruvate (Fig. 1A). Pyruvate is converted into either organic acids, forming the fermentation pathway, or into acetylCoA, forming the starting point for the tricarboxylic acid (TCA) cycle and the respiratory pathway. This raises the question of how the flux at this branch point is regulated during overflow metabolism and how this might relate to the constraint-based view described above. A seminal modelling study showed that branch points could provide a point of regulation, as the distribution of fluxes among the two branches can be readily altered by regulating the levels or catalytic properties of the enzymes catalysing the reactions on each branch [24]. For the pyruvate branch point specifically, enzymes immediately downstream of the branch point, including pyruvate decarboxylase (PDC) on the fermentation branch and pyruvate dehydrogenase (PDH) on the respiration branch, all have identified allosteric, post-transcriptional, or transcriptional regulators [37, 21, 42]. In the case of PDH, for example, altering post-translational regulation of this enzyme is shown to influence metabolic overflow in mammalian cells [25].

Another interesting feature of the pyruvate branch point is the involvement of co-substrates in reactions at or around the branch point, a feature commonly observed across branch points in central metabolism (Fig. 1D). Co-substrates are additional metabolites taking part in a reaction, acting as donors and acceptors of chemical groups or facilitators of enzymatic mechanisms. Key examples include NAD+/NADH and ATP/ADP, which act as electron and phosphate carriers. The concentrations of co-substrates are commonly assumed as constants in metabolic models, but when this assumption is relaxed, co-substrate dynamics can become flux limiting [51, 23, 17, 19, 43]. Potential functional significance of the placement of co-substrate-linked reactions around a branch point, and their impact on flux regulation, are however not explored. Experimentally in yeast and bacteria, modulating NADH dynamics (via introducing enzymes that can consume or produce NADH) is found to change the level of glucose consumption and the growth rate at which metabolic overflow is initiated [48, 47]. These findings lead to the hypothesis that co-substrate dynamics are interlinked with alteration of fluxes at the pyruvate branch during metabolic overflow.

Here, we provide supporting evidence for this hypothesis using mathematical models and experimental measurements from yeast. We first develop minimalistic models of metabolic branch points with different topologies of co-substrate-involving reactions. Analysis of these models shows that co-substrate dynamics can introduce a type of 'self-regulation', where the flux distribution at a branch point can change in a nonlinear fashion, as influx into the upstream pathway increases. We show that this inherent regulation of flux distribution at the branch point arises from asymmetric co-substrate usage, at and around the branch point. A similar effect can be achieved with differential enzyme affinities at the branch point, but the co-substrate based mechanism is less restricted by parameter choices and achieves higher sensitivity. We then develop a more specific model of the pyruvate branch point in yeast, accounting for NADH dynamics across cytosol and mitochondria. We show that mitochondrial NADH dynamics in this model can drive a nonlinear flux switching into fermentation with increasing glucose influx. This model behaviour qualitatively captures experimentally observed shifts in NADH levels during metabolic overflow[6, 16]. The model can also account for how changes in NADH turnover rates alters threshold glucose level for initiating metabolic overflow [48, 47]. We conclude that the co-substrate dynamics around metabolic branch points introduce a flux switching mechanism that acts as a self-regulatory element and that this can explain the overflow metabolism. As a corollary, and in light of the developed predictive theory, we hypothesize that modulating co-substrate dynamics at branch points can allow explanation and engineering of different dynamic behaviours in cell metabolism.

3 Results

Co-substrate-involving reactions (CRs) are commonly found at or around branch points in cell metabolism. We postulate a role of co-substrate dynamics in the distribution of metabolic fluxes at a branch point. While NADH dynamics around the pyruvate branch point constitutes a key example, which we will analyse further below, branch points are common throughout cellular metabolism (Fig. 1). Interestingly, different branch points show different placement of CRs at and around them. For example, the pyruvate branch point in yeast harbours two NADH-linked CRs, one immediately downstream of the branch point, and another one some distance upstream (Fig. 1A). In other examples, the upper glycolysis features CRs involving ATP and NADH (Fig. 1B), while the ammonia assimilation branch point features CRs involving NADH and NADPH (Fig. 1C). Overall, and using the latest genome scale models, we have identified hundreds of metabolic branch points in *Saccharomyces cerevisiae* and *Escherichia coli* [52, 30], many of which are linked to co-substrates (Fig. 1D). How might co-substrate dynamics arising from CRs placed at and around a branch-point influence flux distribution at the branch point?

To explore this question, we focus first on minimalist models of a branch point that can provide a didactic insight. In all analyses, we focus on the steady-state flux fraction into one branch (arbitrarily taken as the upper branch, i.e. $F_f = F_{\text{upper}}/(F_{\text{lower}}+F_{\text{upper}})$) as a key variable describing the pathway dynamics. We consider the branch-point reactions to either be reversible or irreversible, and model these using the established Haldane and Michealis-Menten equations, respectively (see *Methods* and Figure S1). Total co-substrate levels are assumed to be conserved, i.e. the sum of the two forms of the co-substrate (B_0 and B_1) is a constant, B_{T}. In the supplementary information (SI), we show that this assumption can be relaxed without loss of the general results presented here (see SI 5 and Figure S2). The effects of any 'off-pathway' reactions consuming and generating the co-substrate are modelled as a single, enzymatic reversible reaction from B_0 to B_1 with equilibrium coefficient K^B_{eq} and maximal rate V^B_{max}. In the context of NADH, for example, this abstract reaction represents all off-pathway processes consuming or producing NADH, such as the respiratory electron transport chain.

Co-substrate dynamics facilitate switch-like flux regulation at a branch point, in response to increasing pathway flux. A model of a branch point without co-substrates has been considered before [24] (Fig. 2A). Here, we first recover the main result from that study, namely that the steady state F_f at the branch point relates to the ratio of the maximal rates of the two branch enzymes ($V^{23}_{\text{max}}/V^{24}_{\text{max}}$). Additionally, when the two branch point enzymes have the same substrate affinity (i.e. $K^{23}_{\text{M}} = K^{24}_{\text{M}}$), F_f is unaffected by any changes in the upstream pathway influx (Fig. 2A(ii), dotted lines). When the substrate affinity of one of the branch-point enzymes is increased by 100-fold compared to the other (i.e. $K^{23}_{\text{M}} \ll K^{24}_{\text{M}}$), and the same enzyme is set to also have a 10-fold higher maximum rate (i.e. $V^{23}_{\text{max}} \gg V^{24}_{\text{max}}$), we see a nonlinear response of F_f to changes in the upstream pathway influx v_{in} (Fig. 2A(ii), blue solid line). The magnitude of this response can be quantified as the difference of flux fraction at the highest and the lowest influx levels, shown as ΔF_f(Fig. 2A(ii)), while its sensitivity (i.e. degree of response nonlinearity) can be measured by the response gradient (Fig. 2A(iii)). This analysis shows that differences in the kinetics of branch-point enzymes can result in a response of F_f to increasing influx, but this response is highly dependent on parameter choice (Fig. 2A(ii)) and has low sensitivity (Fig. 2A(iii)).

We next consider the case of placing a single CR immediately at the branch point (M_2), utilizing one form of a co-substrate, B_0 (e.g. NADH or NAD^+) (Fig. 2B). Interestingly, changes in the upstream pathway influx rate v_{in} now cause a nonlinear change in F_f (Fig. 2B(ii)), even when both branch-point enzymes have the same kinetic parameters (i.e. $V^{24}_{\text{max}} = V^{23}_{\text{max}}$ and $K^{24}_{\text{M}} = K^{23}_{\text{M}}$; Fig. 2B(ii) olive dotted line). When differences in kinetic parameters of branch-point enzymes are introduced, this enhances the switch-like response in F_f and its sensitivity (Fig. 2B(ii) and (iii), solid lines).

The observed change in F_f coincides with a depletion of one of the co-substrate forms (B_0) as influx increases (Fig. 2B(ii), inset). This depletion introduces an asymmetry between the branch-point reactions in

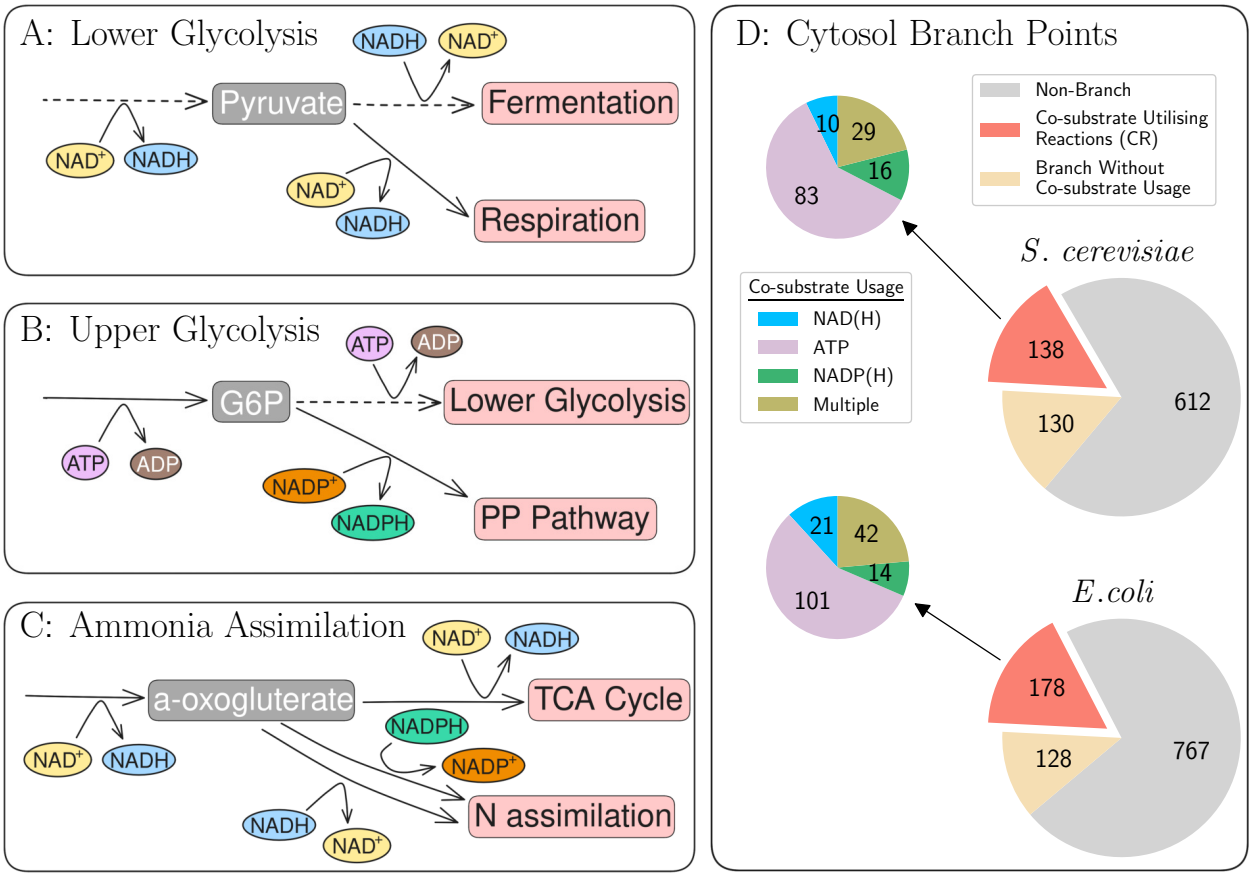

Figure 1: Branch points in central metabolism (A-C) Cartoon representation of different examples of branch points with co-substrate-involving (CR) reactions. Each cartoon is based on corresponding reaction maps included in the Yeast Pathways database [13] and are simplified for tractability. In particular, dashed arrows indicate multiple reactions, grey and red boxes indicate metabolites and processes respectively, and other colours indicate different co-substrates. EC Numbers and pathways used to create the cartoons are: (A) Lower Glycolysis - 1.2.12 (glycolysis I), 1.1.1.1 (superpathway of glucose fermentation), 1.1.1.41/1.1.1.286 (TCA cycle, aerobic respiration). (B) Upper Glycolysis - 2.7.1.1/2.7.1.2 (superpathway of glucose fermentation), 2.7.1.11 (glycolysis I, from glucose 6-phosphate), 1.1.1.49 (pentose phosphate pathway, oxidative branch I). (C) Ammonia Assimilation - 1.1.1.41/1.1.1.286, 1.2.1.- (both from TCA cycle and aerobic respiration), 1.4.1.4 (glutamate biosynthesis from ammonia), 1.4.1.14 (L-glutamate biosynthesis IV). (D) Branch point metabolites using specified co-substrates in *S. cerevisiae* and *E. coli*. Genome-scale models presented in [52] for *S. cerevisiae* and [30] for *E. coli* are analysed for metabolites that are consumed in two or more reactions, excluding excretion reactions. All these metabolites are counted as "branch-point metabolites" and are further analysed for the presence of immediate consuming reactions involving specific co-substrates. Analysis is presented for metabolites in the cytosol with co-substrates ATP and NAD(P)H (and their different forms), as these groups accounted for most of the cases (see also *Methods*).

terms of substrate availability, which can explain the observed F_f response. Compared to the case without a CR, the response generated through co-substrate dynamics does not require specific kinetics of the branch point enzymes (compare Fig. 2A(ii) and B(ii)) and displays a higher sensitivity even for the same parameters (compare Fig. 2A(iii) and B(iii)). We conclude that introducing a CR at the branch point creates an asymmetry and facilitates a form of self-regulation involving a switch-like response in F_f at a threshold level of pathway influx.

Flux switch is affected by asymmetric co-substrate usage across the branch-point. To explore the intuition that flux switch is driven by asymmetric co-substrate usage at the branch point, we quantified the switch response, ΔF_f, in different network structures as a function of key parameters B_{T} or V^B_{max}. We expect that increasing either parameter will increase co-substrate availability in the system, thereby reducing the extent of asymmetry caused by differential co-substrate usage at the branch point. The expected outcome would be that either the switch occurs at a higher influx, or the switch disappears all together. We find that this expectation is realized for both parameters (Fig. 3 and Fig. S4).

We also expect that additional CRs upstream or downstream of the branch point to alter response dynamics in ways that are linked to their effect on the asymmetry of co-substrate usage at the branch point. For example, introducing an upstream (downstream) CR to increase (negate) the asymmetry caused by a CR at the branch point, increases (reduces) the response magnitude (compare Fig. 3A, B and C). Similarly, introducing a second CR at the branch point in a way to reduce asymmetric usage arising from a single CR, reduces the response magnitude for high B_{T} and low V^B_{max} (compare Fig. 3A and D). Adding a further, upstream CR reduces this effect for the same parameter regime and increases the response magnitude again, as it re-introduces asymmetry in co-substrate usage (compare Fig. 3D and E). Finally, if there is only a single CR in the system but is placed upstream or downstream of the branch point (but not at the branch point itself), this should result in symmetry at the branch point dynamics, and hence abolish the switch response. Again, these expectations are realised (Fig. 3F).

In general, we find that, for the case when branch point enzyme K_{M}'s are equal, creating a F_f response to influx requires at least one CR to be at the branch-point, while an upstream CR generally enhances the F_f response (Fig. 3 and Fig. S6). Overall, these results indicate that the introduction of CRs across a branch point provides a flexible mechanism for the introduction of nonlinear flux switching with increasing influx, and that the emergence of this response can be understood from a particular co-substrate becoming limiting at a branch point with asymmetric co-substrate usage.

Another way of breaking substrate-usage symmetry at the branch point would be through allosteric regulation of one of the branch-point enzymes by their substrate. We find that this can introduce a low level of 'self-regulation' in the case without CRs, and can increase the response nonlinearity in the case with CRs (see Figure S3).

A simplified model of co-substrate dynamics at the pyruvate branch point in yeast captures the experimentally observed features of metabolic overflow. The motifs analysed above are similar to those seen in central carbon metabolism (see Fig. 1A). In the case of glycolysis, NAD^+ participates in a reaction upstream,and in a reaction immediately downstream of the pyruvate branch point. In particular, NAD^+ reduction at the pyruvate branch point initiates the respiratory pathway, while NADH is oxidised in the fermentation pathway further downstream (Fig. 1A).

Based on these points, we created here a simplified model of NADH-utilising reactions in the lower part of the yeast glycolysis pathways, around the pyruvate branch point (Fig. 4A). This model takes into account the fact that the pyruvate branch point is split across the cytosol and mitochondria, where pyruvate is transferred into mitochondria before entering the TCA cycle, and crucially, the NADH pools for the cytosol and the mitochondria are separated and possibly connected by mitochondrial shuttles [2]. Given the additional

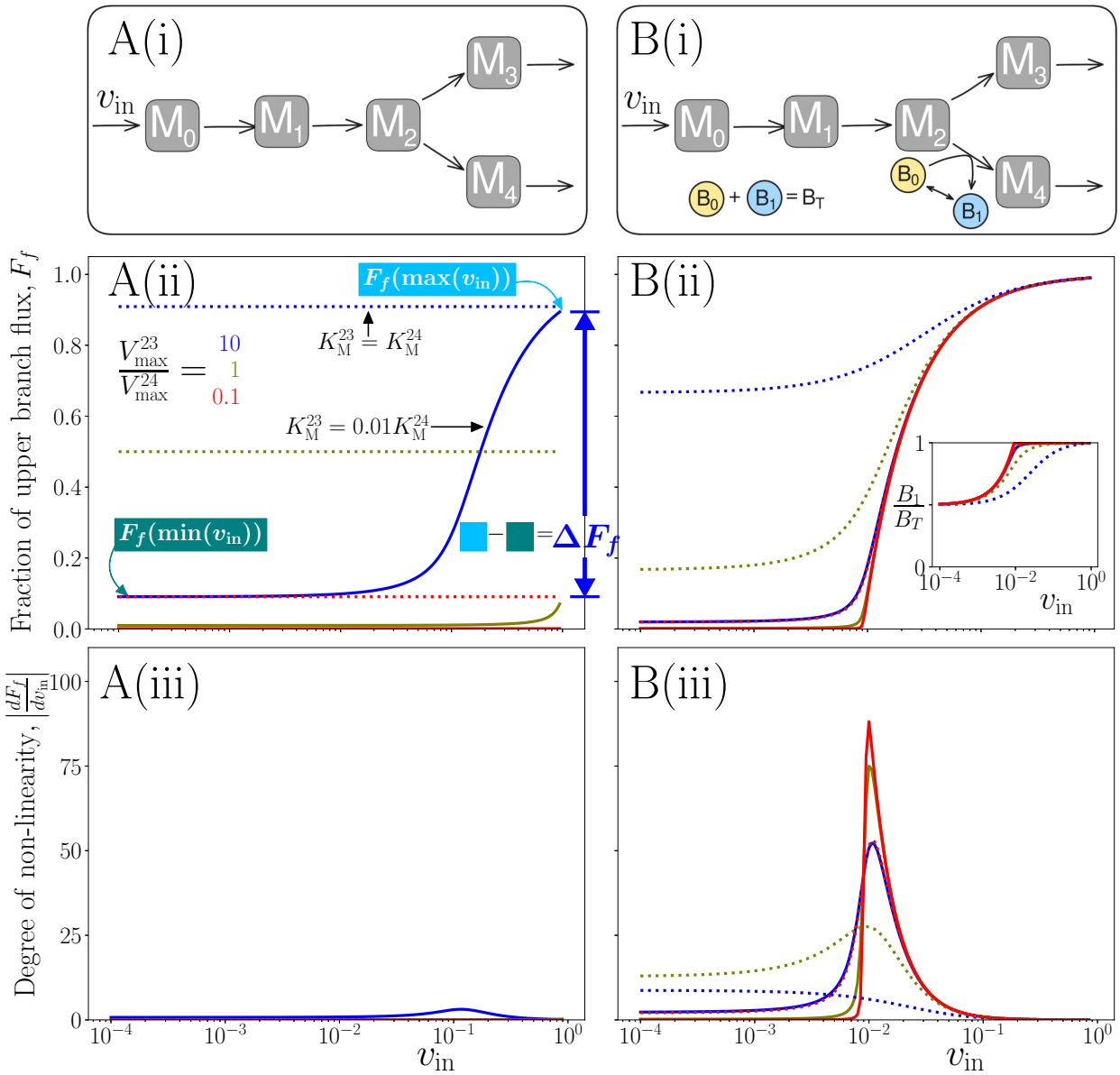

Figure 2: Asymmetric usage of co-substrates across branches enables flux switching when influx exceeds a threshold. (A,B)(i) Simple branch-point motif without co-substrates (A) and a minimal case with co-substrates on only one branch (B). All reactions apart from the background conversion of B_0 and B_1 are modelled as irreversible. (A,B)(ii): Simulation results from models corresponding to the motifs shown in (i) (see Figure S1 for example equations for motif B). Each panel shows the steady state flux fraction, F_f, as the ratio of steady state flux from M_2 to M_3 over total flux at the branch point, against increasing influx into the pathway v_{in}. Blue/olive/red lines indicate when the v_{23} is larger than, equal, or smaller than v_{24}. Dotted lines show the case where $K^{24}_M = K^{23}_M$, while the solid lines show the case for $K^{23}_M = K^{24}_M/100$, with all other parameters set arbitrarily to 1. For panel B, $(B_T, V^B_{max}) = (10, 0.01)$, with all other parameters set arbitrarily to 1, while solid lines show simulation results with the same parameters, except $K^{24}_M = 100$ and insets show the B_1/B_T fraction. (A,B)(iii): Absolute value of the gradient of the flux fraction with respect to v_{in}.

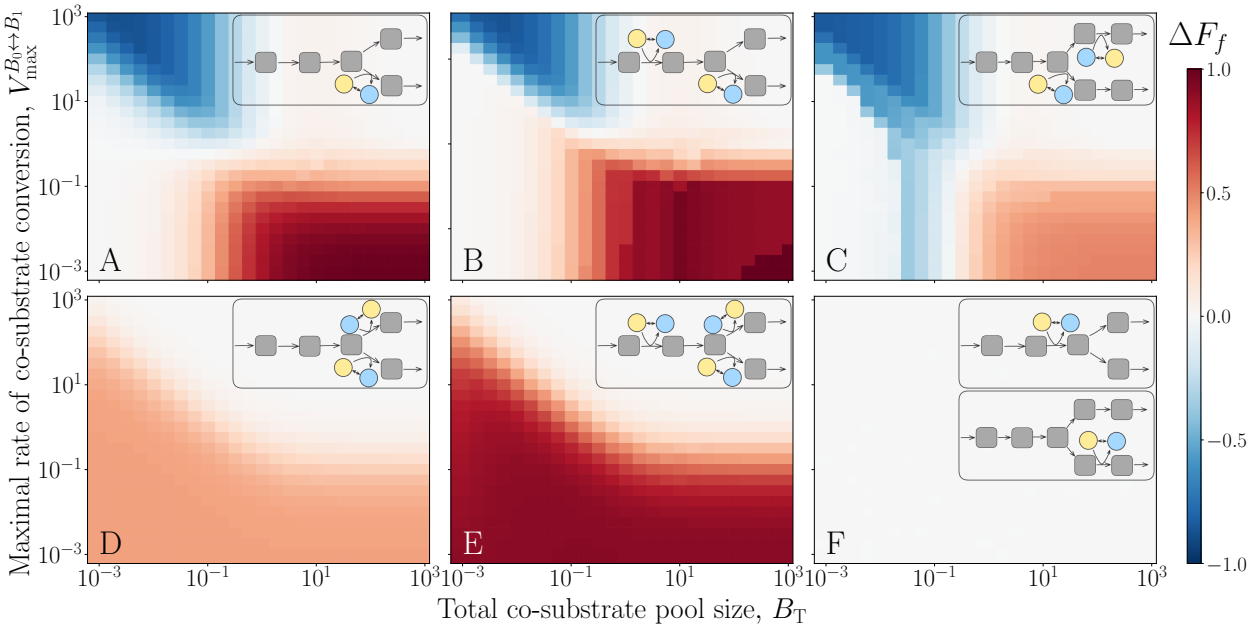

Figure 3: Motif structure influences capacity for regulation. Heatmaps showing $\Delta F_f = F_f(\max(v_{\mathrm{in}})) - F_f(\min(v_{\mathrm{in}}))$ (as shown in Fig 2A(ii)) as a function of B_{T} and $V_{\max}^{B}$ for metabolic motifs with (A) co-substrate on only one branch (similar to Fig. 2B); (B) co-substrates on one branch and upstream in same direction; (C) co-substrate directly on one branch, and downstream on the other branch. (D) co-substrates on both branches in opposite directions; (E) co-substrates on both branches and upstream; (F) co-substrates either downstream (i.e. not directly on) of the branch point or upstream only. Simulations are performed for each combination of B_{T} and $V_{\max}^{B}$ and using $V_{\max}^{23} = 0.1$ (i.e. favouring the bottom branch) and all other parameters set to 1.

features in this more complex model, and specific placement of NADH-involving reactions, we wondered if co-substrate dynamics can still underpin a flux switching (i.e. high ΔF_f) with increasing influx, as seen in the metabolic overflow phenotype observed experimentally (Fig. 4B, see also *Methods*). To parameterise the model, we used *in vitro* determined parameters utilised in previous models of yeast glycolysis [44] where possible, and then performed a sampling approach for other, unknown parameters to cover physiologically relevant ranges [3, 18](see *Methods* and Table S1). For each set of sampled parameters, we simulated the model to obtain F_f response against increasing influx and quantified ΔF_f. We have also quantified any switch-like dynamics in the NADH pool by measuring the extent of change in the fraction of NADH in the cytosol or mitochondria (ΔN_H^m and ΔN_H^c).

We found that the model is capable of flux switching (high ΔF_f), and for some parameter ranges this is accompanied with high ΔN_H^m (Fig. 4D and Fig. S7). The former case does not involve any changes in the co-substrates, indicating that the switching mechanism in these cases does not involve NADH dynamics (Fig. 4F). Indeed, we found that cases of high ΔF_f and zero ΔN_H^m are characterized by high, and opposing, differences in the K_{M} and $V_{\max}$ of the branch point enzymes (Fig. S7C, compare blue vs. pink distributions), conforming to the enzyme-based mechanism noted with the didactic models presented above (Fig. 2A(i). On the other hand, certain cases of high ΔF_f are accompanied by high ΔN_H^m, i.e. show changes in NADH dynamics (Fig. 4E). In particular, the flux switching is preceded by a large switch in the mitochondrial NADH fraction (ΔN_H^m) (Fig. 4E, green and blue lines), while cytosolic NADH fraction does not switch and the total NADH fraction change can be explained by the change in mitochondrial NADH fraction (Fig. 4E, red and orange lines). This indicates that for these cases, the mitochondrial NADH dynamics is the driving factor behind the switching behavior. Supporting this view, we find that for these cases the key parameters underpinning switching relate to co-substrate cycling in the mitochondria (Fig. S7B, compare green vs. pink distributions).

The above findings show that models implementing the specific pathway structure of the yeast pyruvate branch point, and parameterised in a physiologically relevant regime, can display switch-like F_f responses as seen experimentally in metabolic overflow through two distinct mechanisms involving either differential kinetics of pyruvate-consuming enzymes or co-substrate dynamics. Altering the model parameters and structure such that either one of these mechanisms is excluded, high ΔF_f is still possible (Fig. S8). This shows that the two mechanisms can operate independently. We note, however, that only the mechanism involving co-substrate dynamics produces a switch in NADH levels during metabolic overflow, as observed experimentally (Fig. 4E). In particular, whole cell measurements from chemostat experiments with yeast show an abrupt increase in NADH and a decrease in NAD^+ levels after the onset of metabolic overflow [45, 6, 16] (Fig. 4B), as seen in the model (Fig. 4E, red line). In addition, we find that for the models where high ΔF_f is achieved through co-substrate dynamics, altering the recycling dynamics of mitochondrial NADH pools, by shifting the equilibrium dynamics towards NAD^+, results in the shifting of the flux switching point to higher influx levels (Fig. 4E, dashed lines). These observations, as well, match with experimental findings in yeast, showing introduction of foreign NADH-consuming reactions shifting the metabolic overflow initiation point to higher glucose levels [48, 19] (Fig. 4E and S9). We also find that the shifting the equilibrium dynamics towards NADH in the mitochondria in the model results in shifting of the metabolic overflow initiation point to lower glucose levels (Fig. S9D). There is experimental analyses of deletion of NADH-specific mitochondrial dehydrogenases in *S. cerevisiae*, but whether these link to mitochondrial or cytosolic NADH pools is unclear and their effect on metabolic overflow threshold is not well characterised [31].

Overall, these qualitative agreements between the model behaviour and experimental data indicates that asymmetric dynamics arising from NADH-NAD^+ usage at and around the pyruvate branch point is an integral driver of the metabolic overflow dynamics observed in yeast.

4 Discussion

Here, we analysed the flux dynamics at a metabolic branch point, with or without co-substrate-utilising reactions at and around the branch point. Using mathematical models of simple branch point architectures as didactic cases, we shown that (i) differential kinetic paramaters for the branch-point enzymes, or (ii) a specific distribution of co-substrate-utilising reactions as two independent mechanisms enabling flux switching at the branch point with increasing influx. These responses constitute a type of self-regulation, as they do not require active control of enzyme levels or their allosteric regulation and are solely arising from pathway structure and placement of co-substrate reactions. To see how the presented mechanisms could apply to overflow metabolism seen in yeast, we developed a specific model of the pyruvate branch point and the NADH usage around it in yeast. Using measured or physiologically relevant kinetic parameters, we found flux switching response to increasing influx through both mechanisms is possible in this model. However, only co-substrate-based mechanisms are capable of explaining existing experimental data from yeast on NADH and metabolic overflow dynamics, and their influence on each other. Taken together, these findings demonstrate that branch points and co-substrate utilisation around them act as key, 'built-in' regulatory elements within cellular metabolism.

The qualitative agreement between the presented model and yeast metabolic overflow dynamics provides strong support that co-substrate dynamics could influence metabolic overflow. The observed reduction in NAD^+ levels in yeast during metabolic overflow is captured by the co-substrate model. It must be noted, however, that the experimental measurements pertain to the whole cell, rather than mitochondria and cytosol separately, while the model indicates a larger change in mitochondrial NADH dynamics with metabolic overflow initiation. In the case of effects of NADH dynamics on the threshold point for metabolic overflow, the experiments employed both mitochondrial and cytosolic NADH oxidases, and observed only the former to shift the metabolic overflow threshold, as in the presented model (Fig. 4D and S9). These differences in affecting the cytosolic and mitochondrial NADH pools can be understood, in light of the model, due to the lower NADH pool size in the mitochondria, which was shown in mammalian cells [10].

The explanatory power of the presented theory, based on NADH dynamics, can extend to other observations on metabolic overflow in yeast and other species. In this theory, metabolic overflow initiation point is predicted to tightly depend on NADH-NAD^+ turnover rates and pool sizes. Thus, these key physiological parameters in different species or strains, shaped by adaptations to past environmental conditions such as stable or changing oxygen levels [39], can determine their metabolic overflow phenotypes. In this context, we note that recent proteomics studies showed that Crabtree negative yeasts, which have a higher threshold for metabolic overflow, display significantly higher expression levels of electron transport chain enzymes [27, 39]. This suggests a higher mitochondrial NADH recycling in Crabtree negative yeasts, as supported by the finding of higher NAD^+ and lower NADH levels in Crabtree negative vs. positive yeast [39]. The presented theoretical findings also align with the findings from bacteria, where altering of NADH dynamics also resulted in shifting of metabolic overflow initiation point in *Escherichia coli* [47, 48]. In mammalian cells as well, alterations in NADH dynamics are found to affect flux distributions both at the pyruvate branch point, influencing overflow metabolism [25], and downstream at the alpha-ketoglutarate branch point, influencing the induction of reductive glutamine consumption [14]. These diverse finding from different species, all linking to NADH dynamics support the broader notion that co-substrate dynamics act as flux regulators across branch points.

The presented theory provides a clear mechanistic basis on how co-substrate dynamics can affect metabolic flux distributions. As such, it is linked to a series of historic studies proposing a regulatory role for co-substrates [36, 38], including the phenomenological notion of ATP acting an indicator of cellular 'energy charge' [20, 1, 38]. More recent studies have shown that co-substrate dynamics can act as flux limiting [51, 23, 17] and give rise to nonlinear dynamics [19, 43, 38]. The presented work extends these studies by showing a direct nonlinear regulatory effect of co-substrate dynamics around branch points. While we considered here specifically the pyruvate branch point, and NADH dynamics, it is noticeable that key junctions in central metabolism such as the folate cycle, underpinning single carbon transfers, and the TCA cycle, underpinning

nitrogen assimilation, involve branch points and co-substrate usage around them. Thus, future studies can expand the modelling of co-substrate dynamics to specific branch points and also to capturing the interlinked nature of multiple branch points and multiple co-substrates acting on them. There is already experimental findings suggesting, for example, that aerobic glycolysis in mammalian cells involves an interplay between NAD^+-NADH and ATP-ADP dynamics [25].

The dynamical explanation for metabolic overflow we presented here is distinct from those explaining metabolic overflow arising from cells altering their protein investment into fermentative and respiratory pathways, according to the proteome efficiency of these two pathways [29, 4, 22]. Those theories operate at a higher, phenomenological level, and do not provide any mechanistic explanations for how cells sense and initiate such a proteome allocation adjustment and how different species or strains can have different metabolic overflow thresholds [4]. Thus, the presented theory could be complementary to the ideas surrounding protein allocation, as co-substrate-based flux regulation at branch points can act as a fast-acting, self-regulatory response to achieve flux changes, which can then be facilitated further with slow-acting, and longer-term, changes in enzyme allocation. This aligns with experimental findings on metabolic overflow, whereby time-resolved perturbation of dilution rate in a chemostat results in a metabolic overflow within seconds to minutes and transcriptional changes are only observed after adaptation to increased dilution rate [34]. It would, therefore, be interesting to expand ongoing efforts of generating 'coarse-grained' cellular models, based on resource allocation, with the inclusion of co-substrate dynamics and key branch points from central metabolism.

In recent years, attempts are emerging to modulate co-substrate dynamics for direct engineering of cellular metabolism for biotechnological applications [9, 41, 40]. We note that the presented co-substrate-based theory - and extensions of it - can provide a predictive basis for these attempts. In particular, specific modulation of NADH turnover rates can be used to engineer metabolic overflow through the pyruvate branch point. Future application of the presented theory to other branch points, or several connected branch-points, can allow engineering of metabolic fluxes associated with other phenotypes.

5 Methods

Analysis of branch-point motifs in genome-scale models. We used latest genome-scale metabolic models for yeast [52] and *E. coli* [30]. For a given model, we identified those metabolites that are consumed in two or more reactions, excluding excretion reactions but including inter-organelle transport reactions. These metabolites are counted as "branch-point metabolites". We then categorised each branch-point metabolite as involving a CR, if any of its immediate consuming reactions involved co-substrates ATP or NAD(P)H (and their different forms). The analysis was performed for all compartments, but the results are shown only for the cytosol as this group accounted for most of the cases identified. The analysis script, written in MATLAB, as well as the genome-scale models used are available at the Github repository: `https://github.com/OSS-Lab/Co-substrate-induced-flux-switching-at-branch-points-can-explain-overflow-metabolism`

Modeling of branch-point motifs. We used ordinary differential equations to model the dynamics of branch point containing pathways, with and without CRs. In the case of CRs, specific co-substrate forms - generically represented as B_0 and B_1 - are assumed to take part in a given reaction and the total amount of co-substrate is assumed to be fixed (i.e. $B_0 + B_1 = B_\mathrm{T}$), an assumption relaxed in the supplementary material (see Fig. S2). In addition to the CRs directly modelled, a 'background', reversible $B_0 \leftrightarrow B_1$ conversion reaction is implemented to account for reactions not related to the branch-point motif, with an equilibrium coefficient of K^B_eq. All reactions are modelled using single or two-substrate versions of the Michealis-Menten or reversible Haldane reaction rates, assuming simultaneous binding of all substrates to the enzyme. The generic forms of these reactions result in rate equations as shown in Fig. S2.

The resulting reactions and rate equations are incorporated in a series of ODEs for each model and depending on the model architecture. All ODE systems are implemented as a Python script and solved using numerical methods implemented in scipy library. A set of ODEs for an example system (that shown in Fig.

2B) are given in the SI Section **??**, while the main analysis script is made available at the following Github repository: `https://github.com/OSS-Lab/Co-substrate-induced-flux-switching-at-branch-points-can-explain-overflow-metabolism`

Simulation of flux behavior. A key metabolic behavior, we have focused here, is the dynamics of flux distribution at a branch point. To quantify this behaviour, we considered the steady-state flux fraction into the upper branch as a key measure describing the pathway dynamics, ($F_f = F_{\text{upper}}/(F_{\text{lower}}+F_{\text{upper}})$). To get F_f for a given pathway architecture, we simulate the ODEs to steady state for different values of influx rate and record system variables, resulting in a response curve as shown in Fig. 2). For the models used in motif analyses, reaction kinetic parameters are set to arbitrary values for simplicity, with the key parameters, such as K^B_{eq}, B_{T}, and maximal rate of the 'background' $B_0 \leftrightarrow B_1$ conversion reaction varied to assess their effects in system dynamics (as shown in Fig. 2 and Fig.3). These phase plane analyses involve running time-course simulations as described above for different parameters sets, to steady state, and obtaining F_f. Simulated systems are assumed to have reached steady state, when all metabolite gradients are smaller than 10^{-5} after a simulation time of 10^5 minutes.

Yeast pyruvate branch-point model. The simplified model of the lower glycolysis and the pyruvate-branch point shown in yeast are modelled based on a previous model of the lower glycolysis in yeast [44]. The model is simplified by only focusing on the pyruvate branch point, lumping some of the linear parts of the lower glycolysis into a single reaction, and expanding with reactions around the branch point. The model includes the compartmentalisation of NADH across cytosol and mitochondria, resulting in distinct cytosolic and mitochondrial pools, along with NADH-shuttle reactions that are proposed to consume/produce NADH using either of these pools [2]. Transport of pyruvate into mitochondria is modelled and forms, together with the pyruvate decarboxylase mediated reaction in the cytosol, the pyruvate branch point in this model. Kinetic parameters for most reactions are obtained from the previous yeast model [43]. The kinetics of the pyruvate transport dynamics are obtained from measurements with isolated mitochondria [32], while remaining kinetic parameters are obtained from databases [8, 5]. To account for unknown parameters, and allow for variances in measurements, many of the kinetic parameters are further sampled from a wide, physiologically relevant, range, and centered around measured values where available (see Table S1). For the background reaction for NADH turnover, the K^B_{eq} is set to achieve a NAD^+ to NADH ratio of 100, as observed for the yeast cytosol, but also varied as low as 7, as observed for whole cell metabolite measurements [7]. When comparing the model with/without NADH oxidase, the switch point was first calculated for the case without NADH oxidase. This was defined as the value of v_{in} at which the flux fraction crossed the half-way point between the minimum and maximum. Then for the case with NADH oxidase, the same flux fraction value was used to define the switch point. This was to avoid erroneously counting cases where the system reached overflow sooner, but otherwise had the same flux fraction response curve.

Re-analysis of experimental data. Experimental data plotted in Fig 4B was obtained from two consecutive studies that measured metabolite levels across chemostat experiments, including during metabolic overflow initiation [16, 6]. The two studies analysed the same experimental samples [16]. Data points for ethanol production rate were extracted from the graph in Supplementary Figure S6 of [6] using plotdigitizer.com/app. Absolute concentrations of NADH and NAD^+ from LC-MS/MS analysis were extracted from Supplementary Dataset 9 in [16]. Each bar indicates concentrations averaged over 4 experiments conducted at any given dilution rate of a glucose-limited chemostat. As cell growth is limited by the dilution rate in a chemostat reactor, we use dilution rate under glucose limitation as a proxy for metabolite influx rate into glycolysis. Experimental data plotted in Fig 4C (upper panel) was calculated using switch-point dilution rates mentioned in the main text of [47]. Cytosolic perturbation corresponds to the strain AOX, while mitochondrial perturbation corresponds to the strain NOX, described in ([47]). The percentage change for each perturbation was calculated using the switch-point dilution rate of strain CON, described in ([47]), as reference value, and error propagation was used to calculate the error bars for each perturbation.

References

[1] Daniel E. Atkinson. "The Energy Charge of the Adenylate Pool as a Regulatory Parameter. Interaction with Feedback Modifiers". In: *Biochemistry* 7 (1968), pp. 4030–4034. DOI: 10.1021/bi00851a033.

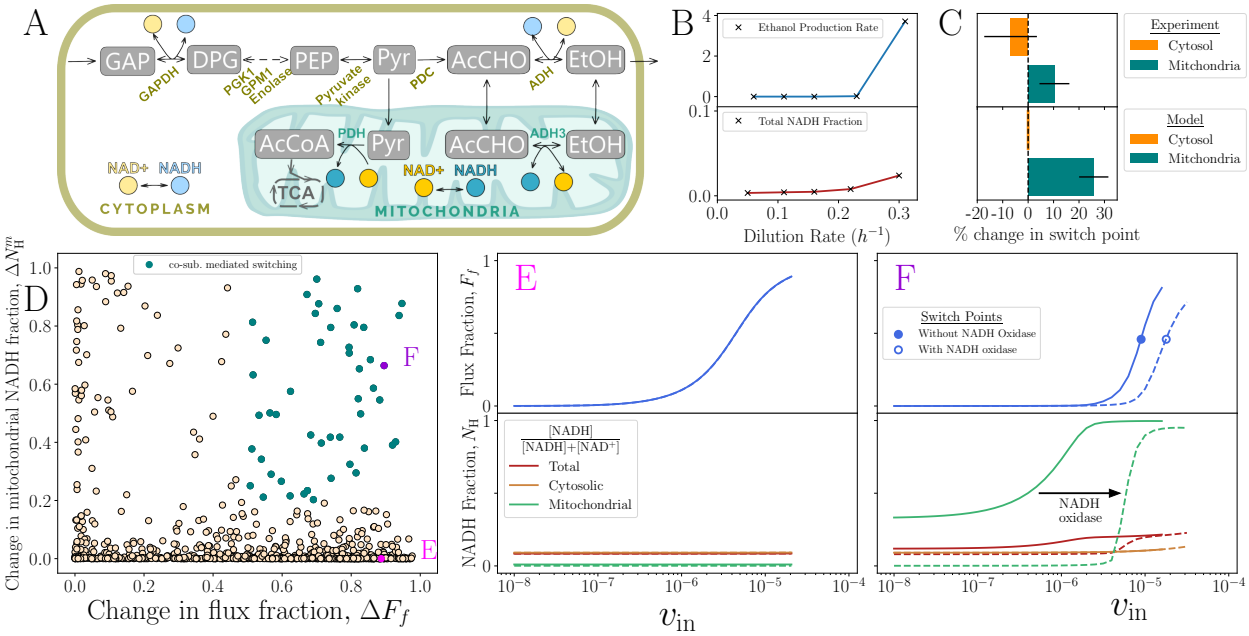

Figure 4: Yeast compartmental model. (A) A cartoon of the pyruvate branch point in yeast, where specific reactions are labelled with the relevant enzyme. Dashed reaction line indicates that multiple reactions have been condensed into one. (B) Experimental data from [6], showing an increase in ethanol production rate and total (i.e. cell-wide) NADH fraction from absolute concentrations in [16]. (C) Box plots showing the % change in switch point position as a result of NADH oxidases in different cell compartments. Experimental data is from [47]. NADH oxidase is incorporated into the model by reducing K_{eq}^{B} (i.e. biasing the background reaction away from production of NADH). (D) Scatter plot of ΔF_f vs. ΔN_{H}^{m} (change in mitochondrial [NADH]/([NAD$^+$]+[NADH]) fraction). Each point shows simulation results for the model simulated using parameters drawn from the ranges shown in Table S1. Purple/pink dots indicate the points plotted in (E/F), teal dots show the points when calculating the % change in switch point for the model, shown in (C). (E/F) Plot of v_{in} vs flux fraction and co-substrate fraction for the model simulated with specific parameter values, picked from those sampled in (D). The corresponding points are also indicated in (D). Solid lines are simulation results for the original parameter set, while the dashed lines show results from a simulation with the NADH background reaction equilibrium coefficient K_{eq}^{B} reduced by a factor of 10 to favor NAD$^+$, mimicking the experimental manipulation of NADH dynamics with a NADH-consuming oxidase. Blue dots indicate the switch-point used in calculations.

[2] Barbara M. Bakker et al. "Stoichiometry and compartmentation of NADH metabolism in Saccharomyces cerevisiae". In: *FEMS Microbiology Reviews* 25 (2001), pp. 15–37. DOI: 10.1016/S0168-6445(00)00039-5.

[3] A. Bar-Even et al. "The moderately efficient enzyme: evolutionary and physicochemical trends shaping enzyme parameters". In: *Biochemistry* 50.21 (2011), pp. 4402–10. ISSN: 1520-4995 (Electronic) 0006-2960 (Linking). DOI: 10.1021/bi2002289.

[4] M. Basan et al. "Overflow metabolism in Escherichia coli results from efficient proteome allocation". In: *Nature* 528.7580 (2015), pp. 99–104. ISSN: 1476-4687 (Electronic) 0028-0836 (Linking). DOI: 10.1038/nature15765.

[5] M. E. Beber et al. "eQuilibrator 3.0: a database solution for thermodynamic constant estimation". In: *Nucleic Acids Res* 50.D1 (2022), pp. D603–D609. ISSN: 1362-4962 (Electronic) 0305-1048 (Print) 0305-1048 (Linking). DOI: 10.1093/nar/gkab1106.

[6] V. M. Boer et al. "Growth-limiting intracellular metabolites in yeast growing under diverse nutrient limitations". In: *Mol Biol Cell* 21.1 (2010), pp. 198–211. ISSN: 1939-4586 (Electronic) 1059-1524 (Print) 1059-1524 (Linking). DOI: 10.1091/mbc.e09-07-0597.

[7] André B. Canelas, Walter M. Van Gulik, and Joseph J. Heijnen. "Determination of the cytosolic free NAD/NADH ratio in Saccharomyces cerevisiae under steady-state and highly dynamic conditions". In: *Biotechnology and Bioengineering* 100 (2008), pp. 734–743. DOI: 10.1002/bit.21813.

[8] A. Chang et al. "BRENDA, the ELIXIR core data resource in 2021: new developments and updates". In: *Nucleic Acids Res* 49.D1 (2021), pp. D498–D508. ISSN: 1362-4962 (Electronic) 0305-1048 (Print) 0305-1048 (Linking). DOI: 10.1093/nar/gkaa1025.

[9] R. Chen et al. "Engineering cofactor supply and recycling to drive phenolic acid biosynthesis in yeast". In: *Nat Chem Biol* 18.5 (2022), pp. 520–529. ISSN: 1552-4469 (Electronic) 1552-4450 (Linking). DOI: 10.1038/s41589-022-01014-6.

[10] W. W. Chen et al. "Absolute Quantification of Matrix Metabolites Reveals the Dynamics of Mitochondrial Metabolism". In: *Cell* 166.5 (2016), 1324–1337 e11. ISSN: 1097-4172 (Electronic) 0092-8674 (Linking). DOI: 10.1016/j.cell.2016.07.040.

[11] V. Chubukov et al. "Transcriptional regulation is insufficient to explain substrate-induced flux changes in Bacillus subtilis". In: *Mol Syst Biol* 9 (2013), p. 709. ISSN: 1744-4292 (Electronic) 1744-4292 (Linking). DOI: 10.1038/msb.2013.66.

[12] R. Diaz-Ruiz et al. "Tumor cell energy metabolism and its common features with yeast metabolism". In: *Biochim Biophys Acta* 1796.2 (2009), pp. 252–65. ISSN: 0006-3002 (Print) 0006-3002 (Linking). DOI: 10.1016/j.bbcan.2009.07.003.

[13] S. R. Engel et al. "Saccharomyces Genome Database: advances in genome annotation, expanded biochemical pathways, and other key enhancements". In: *Genetics* 229.3 (2025). ISSN: 1943-2631 (Electronic) 0016-6731 (Print) 0016-6731 (Linking). DOI: 10.1093/genetics/iyae185.

[14] E. Gaude et al. "NADH Shuttling Couples Cytosolic Reductive Carboxylation of Glutamine with Glycolysis in Cells with Mitochondrial Dysfunction". In: *Mol Cell* 69.4 (2018), 581–593 e7. ISSN: 1097-4164 (Electronic) 1097-2765 (Print) 1097-2765 (Linking). DOI: 10.1016/j.molcel.2018.01.034.

[15] A. Goel et al. "Protein costs do not explain evolution of metabolic strategies and regulation of ribosomal content: does protein investment explain an anaerobic bacterial Crabtree effect?" In: *Mol Microbiol* 97.1 (2015), pp. 77–92. ISSN: 1365-2958 (Electronic) 0950-382X (Linking). DOI: 10.1111/mmi.13012.

[16] S. R. Hackett et al. "Systems-level analysis of mechanisms regulating yeast metabolic flux". In: *Science* 354.6311 (2016). ISSN: 1095-9203 (Electronic) 0036-8075 (Print) 0036-8075 (Linking). DOI: 10.1126/science.aaf2786.

[17] T. S. Hatakeyama and C. Furusawa. "Metabolic dynamics restricted by conserved carriers: Jamming and feedback". In: *PLoS Comput Biol* 13.11 (2017), e1005847. ISSN: 1553-7358 (Electronic) 1553-734X (Linking). DOI: 10.1371/journal.pcbi.1005847.

[18] C. Hayes, E. Feliu, and O. S. Soyer. "Multisite Enzymes as a Mechanism for Bistability in Reaction Networks". In: *ACS Synth Biol* 11.2 (2022), pp. 596–607. ISSN: 2161-5063 (Electronic) 2161-5063 (Linking). DOI: 10.1021/acssynbio.1c00272.

[19] J. H. van Heerden et al. "Lost in transition: start-up of glycolysis yields subpopulations of nongrowing cells". In: *Science* 343.6174 (2014), p. 1245114. ISSN: 1095-9203 (Electronic) 0036-8075 (Linking). DOI: 10.1126/science.1245114.

[20] J. S. Hofmeyr and A. Cornish-Bowden. "Regulating the cellular economy of supply and demand". In: *FEBS Lett* 476.1-2 (2000), pp. 47–51. ISSN: 0014-5793 (Print) 0014-5793 (Linking). DOI: 10.1016/s0014-5793(00)01668-9.

[21] A. Klyuyeva et al. "Tissue-specific kinase expression and activity regulate flux through the pyruvate dehydrogenase complex". In: *J Biol Chem* 294.3 (2019), pp. 838–851. ISSN: 1083-351X (Electronic) 0021-9258 (Print) 0021-9258 (Linking). DOI: 10.1074/jbc.RA118.006433.

[22] M. A. Kukurugya, S. Rosset, and D. V. Titov. "The Warburg Effect is the result of faster ATP production by glycolysis than respiration". In: *Proc Natl Acad Sci U S A* 121.46 (2024), e2409509121. ISSN: 1091-6490 (Electronic) 0027-8424 (Print) 0027-8424 (Linking). DOI: 10.1073/pnas.2409509121.

[23] H. Kurata. "Self-replenishment cycles generate a threshold response". In: *Sci Rep* 9.1 (2019), p. 17139. ISSN: 2045-2322 (Electronic) 2045-2322 (Linking). DOI: 10.1038/s41598-019-53589-1.

[24] D. C. LaPorte, K. Walsh, and Jr. Koshland D. E. "The branch point effect. Ultrasensitivity and subsensitivity to metabolic control". In: *J Biol Chem* 259.22 (1984), pp. 14068–75. ISSN: 0021-9258 (Print) 0021-9258 (Linking).

[25] A. Luengo et al. "Increased demand for NAD(+) relative to ATP drives aerobic glycolysis". In: *Mol Cell* 81.4 (2021), 691–707.e6. ISSN: 1097-2765 (Print) 1097-2765. DOI: 10.1016/j.molcel.2020.12.012.

[26] R. A. Majewski and M. M. Domach. "Simple constrained-optimization view of acetate overflow in E. coli". In: *Biotechnol Bioeng* 35.7 (1990), pp. 732–8. ISSN: 0006-3592 (Print) 0006-3592 (Linking). DOI: 10.1002/bit.260350711.

[27] C. Malina et al. "Adaptations in metabolism and protein translation give rise to the Crabtree effect in yeast". In: *Proceedings of National Academy of Sciences* 118.51 (2021), e2112836118. DOI: https://doi.org/10.1073/pnas.2112836118.

[28] E. Metzl-Raz et al. "Principles of cellular resource allocation revealed by condition-dependent proteome profiling". In: *Elife* 6 (2017). ISSN: 2050-084X (Electronic) 2050-084X (Linking). DOI: 10.7554/eLife.28034.

[29] D. Molenaar et al. "Shifts in growth strategies reflect tradeoffs in cellular economics". In: *Mol Syst Biol* 5 (2009), p. 323. ISSN: 1744-4292 (Electronic) 1744-4292 (Linking). DOI: 10.1038/msb.2009.82.

[30] J. M. Monk et al. "iML1515, a knowledgebase that computes Escherichia coli traits". In: *Nat Biotechnol* 35.10 (2017), pp. 904–908. ISSN: 1546-1696 (Electronic) 1087-0156 (Print) 1087-0156 (Linking). DOI: 10.1038/nbt.3956.

[31] K. M. Overkamp et al. "In vivo analysis of the mechanisms for oxidation of cytosolic NADH by Saccharomyces cerevisiae mitochondria". In: *J Bacteriol* 182.10 (2000), pp. 2823–30. ISSN: 0021-9193 (Print) 1098-5530 (Electronic) 0021-9193 (Linking). DOI: 10.1128/JB.182.10.2823-2830.2000.

[32] G. Paradies and S. Papa. "On the kinetics and substrate specificity of the pyruvate translocator in rat liver mitochondria". In: *Biochim Biophys Acta* 462.2 (1977), pp. 333–46. ISSN: 0006-3002 (Print) 0006-3002 (Linking). DOI: 10.1016/0005-2728(77)90132-3.

[33] K. Peebo et al. "Proteome reallocation in Escherichia coli with increasing specific growth rate". In: *Mol Biosyst* 11.4 (2015), pp. 1184–93. ISSN: 1742-2051 (Electronic) 1742-2051 (Linking). DOI: 10.1039/c4mb00721b.

[34] M. Petrik, O. Kaeppeli, and A. Fiechter. "An expanded concept for the glucose effect in the yeast Saccharomyces uvarum: Involvement of short- and long-term regulation". In: *Journal of General Microbiology* 129 (1983), pp. 43–49.

[35] T. Pfeiffer, S. Schuster, and S. Bonhoeffer. "Cooperation and Competition in the Evolution of ATP-Producing Pathways". In: *Science* 292.5516 (2001), pp. 504–7. DOI: 10.1126/science.1058079.

[36] J. G. Reich and Evgeniĭ Evgenevich Selkov. *Energy metabolism of the cell : a theoretical treatise*. London ; New York: Academic Press, 1981, viii, 345 p. ISBN: 0125859201.

[37] A. Y. Robin et al. "Deciphering Evolutionary Trajectories of Lactate Dehydrogenases Provides New Insights into Allostery". In: *Mol Biol Evol* 40.10 (2023). ISSN: 1537-1719 (Electronic) 0737-4038 (Print) 0737-4038 (Linking). DOI: 10.1093/molbev/msad223.

[38] E. E. Sel'kov. "Stabilization of energy charge, generation of oscillations and multiple steady states in energy metabolism as a result of purely stoichiometric regulation". In: *Eur J Biochem* 59.1 (1975), pp. 151–7. ISSN: 0014-2956 (Print) 0014-2956 (Linking). DOI: 10.1111/j.1432-1033.1975.tb02436.x.

[39] Y. Shen et al. "Mitochondrial ATP generation is more proteome efficient than glycolysis". In: *Nat Chem Biol* 20.9 (2024), pp. 1123–1132. ISSN: 1552-4469 (Electronic) 1552-4450 (Linking). DOI: 10.1038/s41589-024-01571-y.

[40] A. Shi et al. "Activating transhydrogenase and NAD kinase in combination for improving isobutanol production". In: *Metab Eng* 16 (2013), pp. 1–10. ISSN: 1096-7184 (Electronic) 1096-7176 (Linking). DOI: 10.1016/j.ymben.2012.11.008.

[41] H. S. Song et al. "Enhanced isobutanol production by co-production of polyhydroxybutyrate and co-factor engineering". In: *J Biotechnol* 320 (2020), pp. 66–73. ISSN: 1873-4863 (Electronic) 0168-1656 (Linking). DOI: 10.1016/j.jbiotec.2020.06.017.

[42] M. Spinka et al. "Significance of Individual Residues at the Regulatory Site of Yeast Pyruvate Decarboxylase for Allosteric Substrate Activation". In: *Biochemistry* 56.9 (2017), pp. 1285–1298. ISSN: 1520-4995 (Electronic) 0006-2960 (Linking). DOI: 10.1021/acs.biochem.6b01158.

[43] B. Teusink et al. "The danger of metabolic pathways with turbo design". In: *Trends Biochem Sci* 23.5 (1998), pp. 162–9. ISSN: 0968-0004 (Print) 0968-0004 (Linking). DOI: 10.1016/s0968-0004(98)01205-5.

[44] Bas Teusink et al. "Can yeast glycolysis be understood in terms of in vitro kinetics of the constituent enzymes? Testing biochemistry". In: *European Journal of Biochemistry* 267 (2000), pp. 5313–5329.

[45] P. Van Hoek, J. P. Van Dijken, and J. T. Pronk. "Effect of specific growth rate on fermentative capacity of baker's yeast". In: *Appl Environ Microbiol* 64.11 (1998), pp. 4226–33. ISSN: 0099-2240 (Print) 1098-5336 (Electronic) 0099-2240 (Linking). DOI: 10.1128/AEM.64.11.4226-4233.1998.

[46] M. G. Vander Heiden, L. C. Cantley, and C. B. Thompson. "Understanding the Warburg effect: the metabolic requirements of cell proliferation". In: *Science* 324.5930 (2009), pp. 1029–33. ISSN: 0036-8075 (Print) 0036-8075. DOI: 10.1126/science.1160809.

[47] G. N. Vemuri et al. "Overflow metabolism in Escherichia coli during steady-state growth: transcriptional regulation and effect of the redox ratio". In: *Appl Environ Microbiol* 72.5 (2006), pp. 3653–61. ISSN: 0099-2240 (Print) 0099-2240 (Linking). DOI: 10.1128/AEM.72.5.3653-3661.2006.

[48] G. N. Vemuri et al. "Increasing NADH oxidation reduces overflow metabolism in Saccharomyces cerevisiae". In: *Proc Natl Acad Sci U S A* 104.7 (2007), pp. 2402–7. ISSN: 0027-8424 (Print) 0027-8424 (Linking). DOI: 10.1073/pnas.0607469104.

[49] Thomas Walther et al. "Control of ATP homeostasis during the respiro-fermentative transition in yeast". In: *Mol Syst Biol* 6 (2010). DOI: 10.1038/msb.2009.100.

[50] O. Warburg. "On the origin of cancer cells". In: *Science* 123.3191 (1956), pp. 309–14. ISSN: 0036-8075 (Print) 0036-8075 (Linking). DOI: 10.1126/science.123.3191.309.

[51] R. West et al. "Dynamics of co-substrate pools can constrain and regulate metabolic fluxes". In: *Elife* 12 (2023). ISSN: 2050-084X (Electronic) 2050-084X (Linking). DOI: 10.7554/eLife.84379.

[52] C. Zhang et al. "Yeast9: a consensus genome-scale metabolic model for S. cerevisiae curated by the community". In: *Mol Syst Biol* 20.10 (2024), pp. 1134–1150. ISSN: 1744-4292 (Electronic) 1744-4292 (Linking). DOI: 10.1038/s44320-024-00060-7.

Supplemental Materials: Asymmetric co-substrate usage at a metabolic branch point can drive overflow metabolism

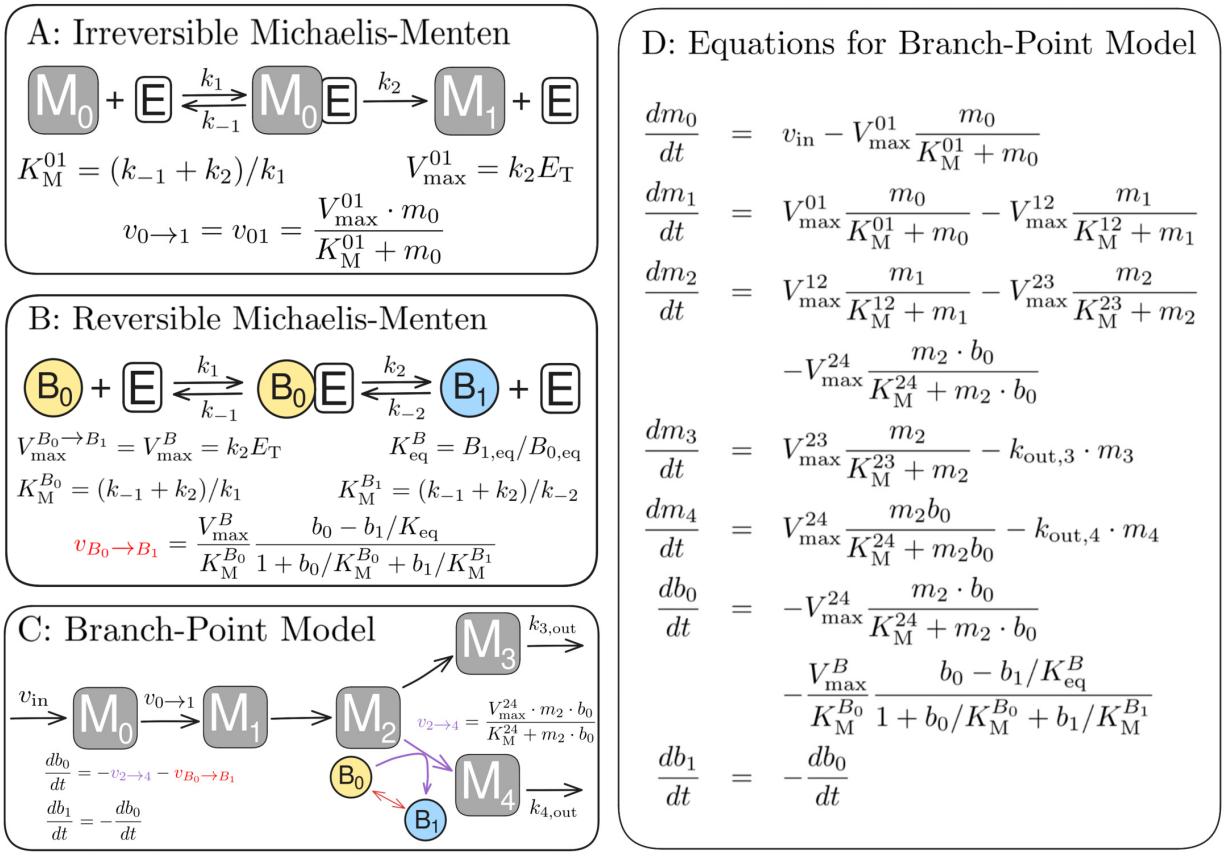

Figure S1: Chemical Reaction Modelling (A,B) Motifs and parameters of the rates used for irreversible and reversible Michaelis-Menten reactions. $M_{0,1}, B_{0,1}$, and E represent metabolites, co-substrates and enzymes respectively; k_1, k_2, k_{-1}, and k_{-2} are binding/unbinding rates, V_{max} is the limiting rate approached by the reaction for large substrate concentrations, K_M is the Michaelis-Menten constant (specific to the reaction and the metabolite) and K_{eq} is the equilibrium constant for the specified reaction (i.e. the ratio of product vs substrate when the reaction has reached state). (C) Schematic for the branch point model showing and example of an irreversible reaction with co-substrates. Here we assume that the substrate, product and their associated co-substrate bind/unbind simultaneously, resulting in the reaction rate being the same as for single substrate reactions, with m_0 replaced by $m_0 b_0$. Additionally, v_{in} is the pathway influx rate, and k_{out} is the outflux rate of the specified metabolite. (D) Example reactions for the branch point model with one co-substrate, as in panel (C) and Fig. 2B. Others can be derived using the same rules. Glucose intake is modelled at a constant rate v_{in}, outflow of the metabolites at the end of each branch as linear, reactions with a single-sided arrow as irreversible Michaelis-Menten, and reactions with a double-arrow as reversible Michaelis-Menten.

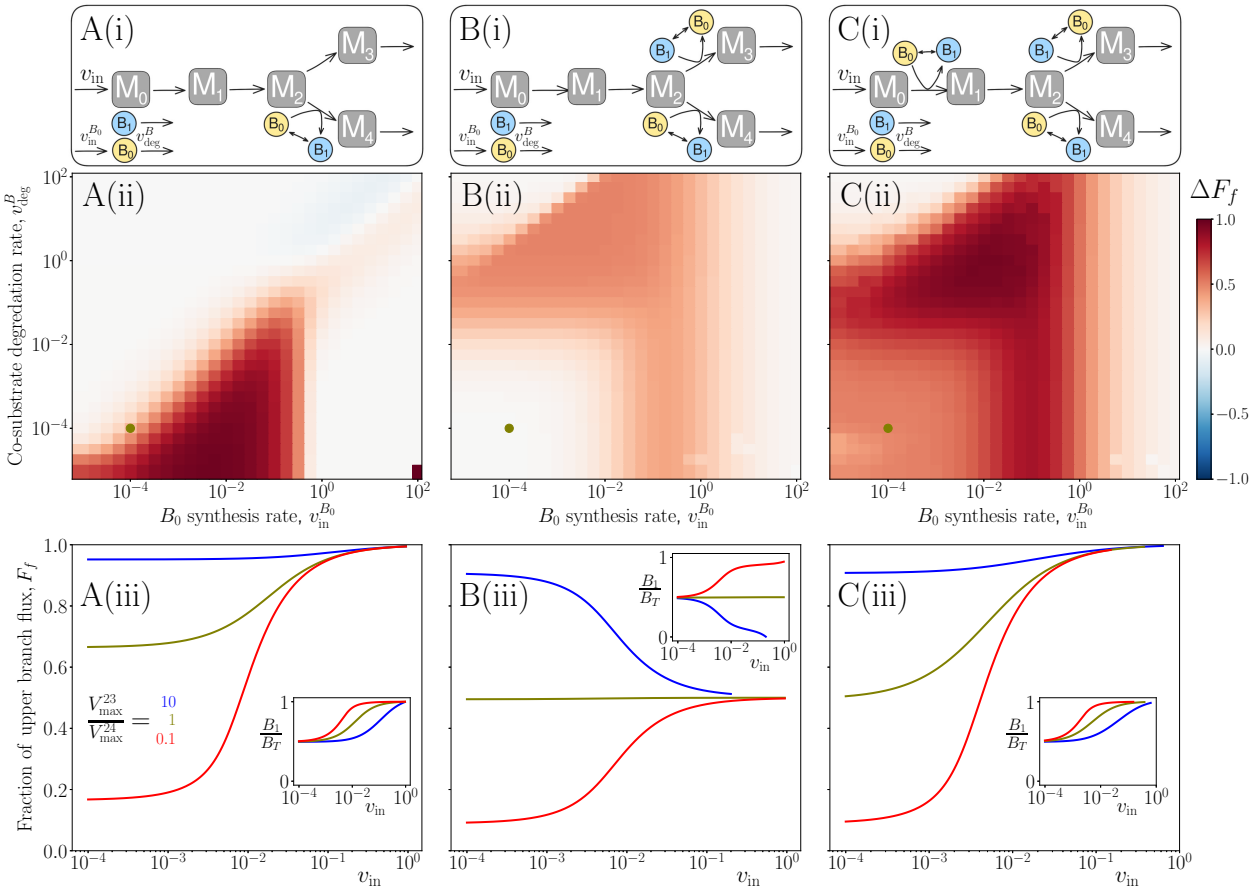

Figure S2: Regulation persists in the presence of synthesis and degredation of co-substrates. (A-C)(i): Simple branch-point motifs with co-substrates on only one branch (A), on both branches (B), and on both the branches and upstream (C). All reactions apart from the background conversion of B_0 and B_1 are modelled as irreversible. (A-C)(ii): Heatmaps showing $\Delta F_f = F_f(\min(v_{\rm in})) - F_f(\max(v_{\rm in}))$ as functions of $v^{B_0}_{\rm in}$ and $v^B_{\rm deg}$ for the metabolic systems in the panels above. $(B_{\rm T}(t=0), V^B_{\rm max}) = (10, 0.01)$, and all other parameters are set arbitrarily to 1 (A-C)(iii): Simulation results from models corresponding to the motifs shown in A-D. Each panel shows the steady-state flux fraction from M_2 to M_4 versus the influx into the pathway $v_{\rm in}$. Red,olive and blue lines indicate conditions favouring the lower branch, neither branch or the upper branch, respectively. Parameters are the same as in the panels above, with $(v^{B_0}_{\rm in}, v^B_{\rm deg})$ corresponding to the olive dot, $V^{24}_{\rm max}$ is shown in the legend, and all other parameters are set arbitrarily to 1. Insets in (A-C)(iii) show the $B_1/B_{\rm T}$ fraction, with the different colored lines showing simulation results with parameters as in the main panel.

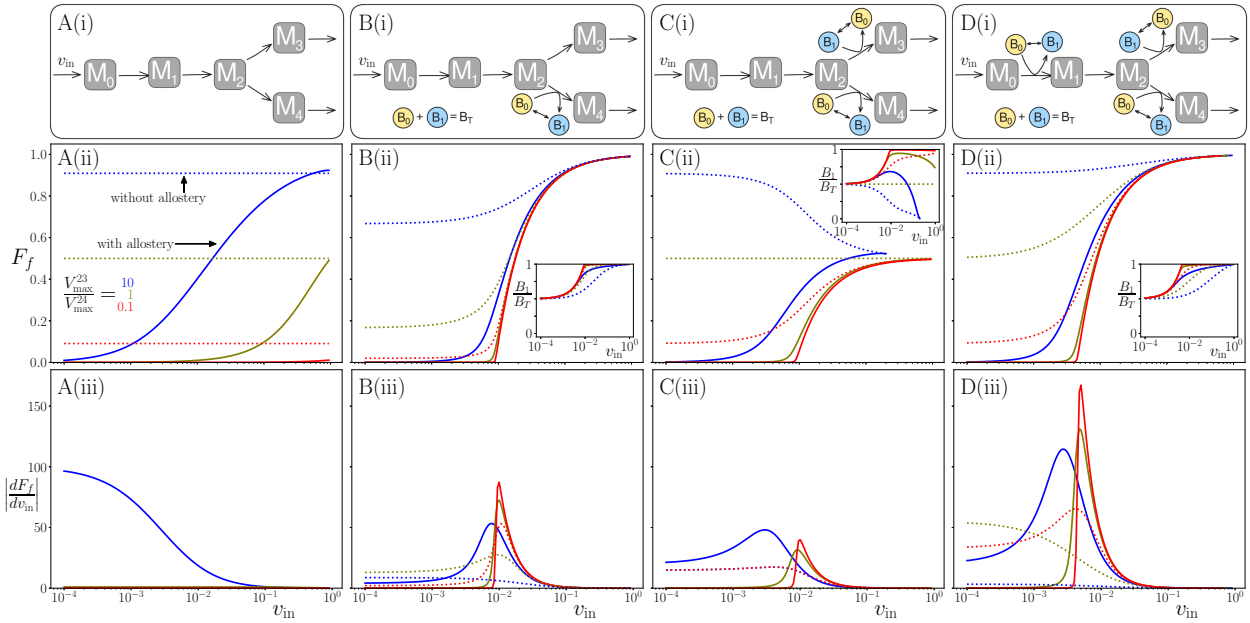

Figure S3: Allosteric regulation enhances nonlinear flux switching at branch points. (A-D)(i): Simple branch-point motifs without (A) and with co-substrates on only one branch (B), on both branches (C), and on both the branches and upstream (D). All reactions apart from the background conversion of B_0 and B_1 are modelled as irreversible. (A-D)(ii): Simulation results corresponding to the motifs shown in (A-D)(i) and modelled without or with allosteric regulation of the $M_2 \rightarrow M_4$ reaction by its substrate (M_2). Each panel shows the steady-state flux fraction from M_2 to M_4 versus the influx into the pathway v_{in}. Red/olive/blue lines indicate when the v_{24}/neither/v_{23} reaction is favoured (legend in A(ii) also applies for all other panels). Dashed lines show the case for $(B_{\text{T}}, V^{B}_{\max}) = (10, 0.01)$ with all other parameters set arbitrarily to 1, solid lines are the same except the $M_2 \rightarrow M_4$ reaction is now modelled to have allosteric regulation by M_2. Allosteric regulation is modelled by using $(m_2)^2$ and $(K^{24}_{\text{M}})^2$ instead of m_2 and K^{24}_{M} in the Michaelis-Menten equation for this reaction. Insets in (A-D)(ii) show the B_1/B_{T} fraction, with the different colored lines showing simulation results with parameters as in the main panel. (A-D)(iii): Absolute value of the gradient of the flux fraction with respect to v_{in}.

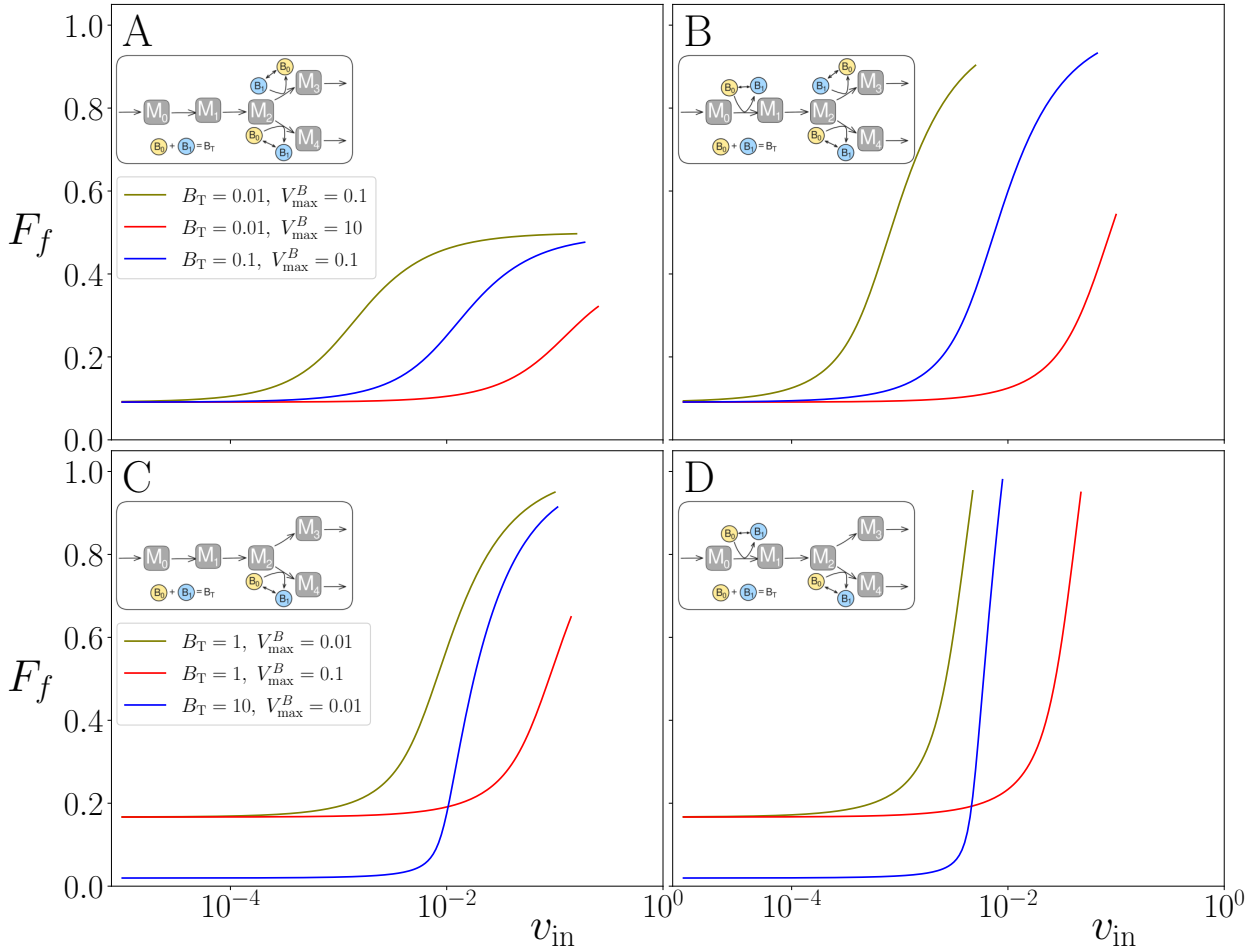

Figure S4: Impact of co-substrate pool size on switching dynamics. Flux fraction versus $v_{\rm in}$ for the motifs shown in the insets, which are the same as in Fig. 3. Legend in panel A applies to both panels A and B, and the legend in C applies to both panels C and D.

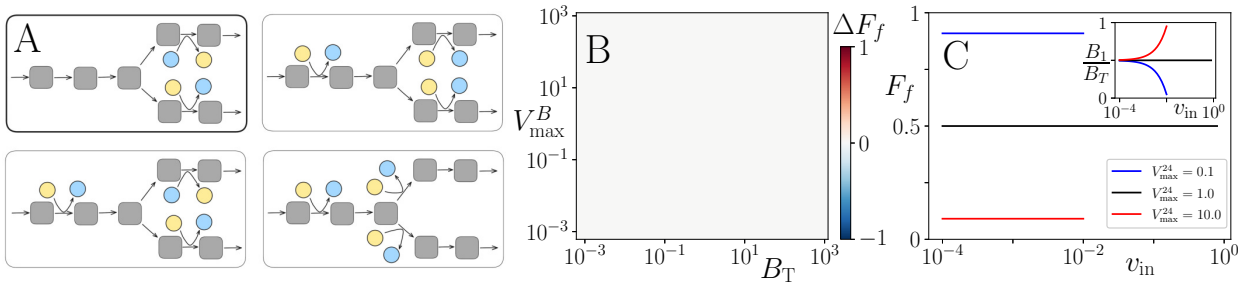

Figure S5: Off-pathway or symmetric co-substrate usage does not result in regulation. (A): Motifs showing placement of CRs around metabolic branch points that do not result in regulation as $v_{\rm in}$ varies (B) Heatmap of ΔF_f as a function of $B_{\rm T}$ and $V^B_{\rm max}$ for the motif with the bold outline in A. $(K^B_{\rm eq}, V^{24}_{\rm max}) = (0.1, 0.1)$, with all other parameters set to 1. (C) Flux fraction versus $v_{\rm in}$ for $(B_{\rm T}, V^B_{\rm max}) = (10, 0.01)$, $V^{24}_{\rm max}$ as indicated in the legend and all other parameters set to 1.

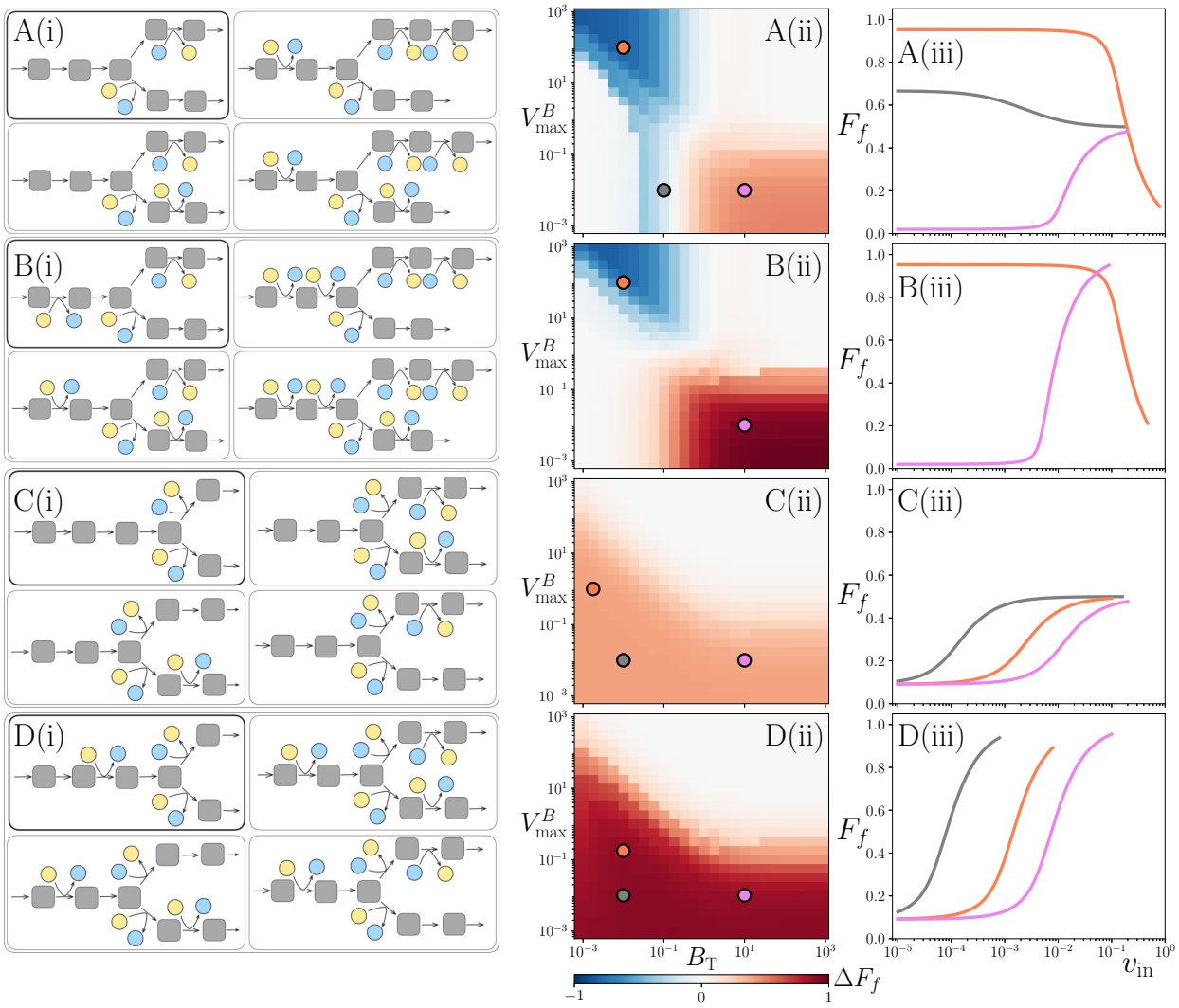

Figure S6: Categorisation of regulation types and associated motifs. (A-D)(i): Motifs exhibiting similar regulation, showing the adjacent heatmap. (A-D)(ii): Heatmaps showing $\Delta F_f = F_f(\min(v_{\text{in}})) - F_f(\max(v_{\text{in}}))$ for bold motif in adjacent panel. All other motifs in each panel have similar heatmaps. $V^{23}_{\max} = 0.1$ (top branch $V_{\max}$) and all other parameters set to 1. (A-D)(iii): Flux fraction vs. v_{in} for the bold motif in the same row, with parameters corresponding to the dots in the adjacent heatmaps.

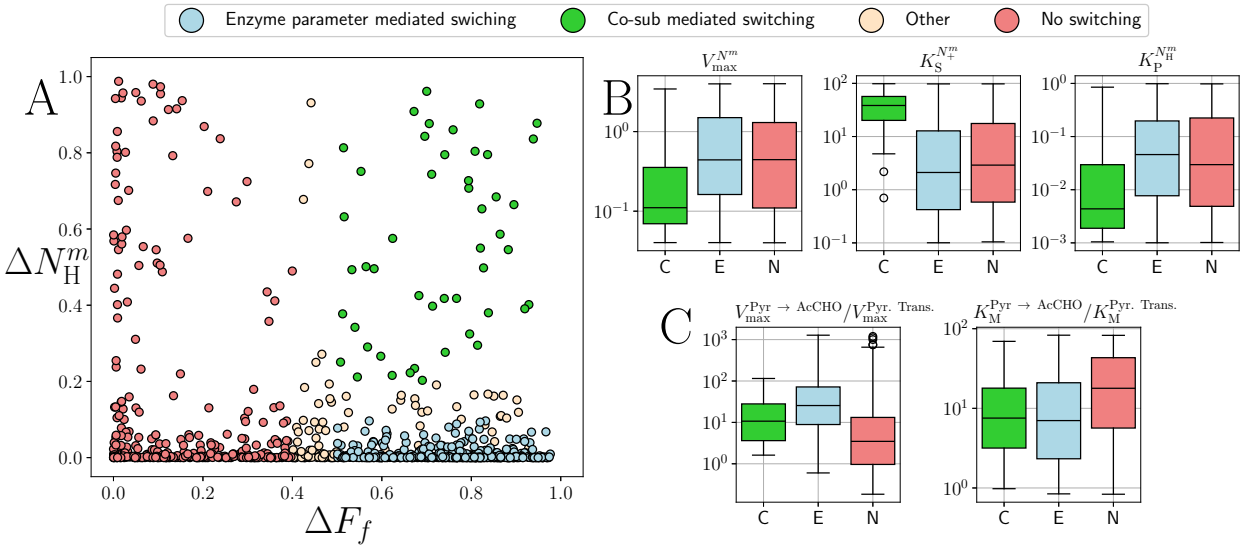

Figure S7: Comparison of parameter regimes in the compartment model (A) Scatter plot of ΔF_f vs. ΔN_{H}^m for the same parameter set as in Fig 4(C), with regions labelled (see legend). (B/C) Box plots showing important parameter regimes for the different switching cases. Colour of box plots shows the points from (A) used. (B) Parameters important for co-substrate mediated switching, (C) parameters important for enzyme mediated switching.

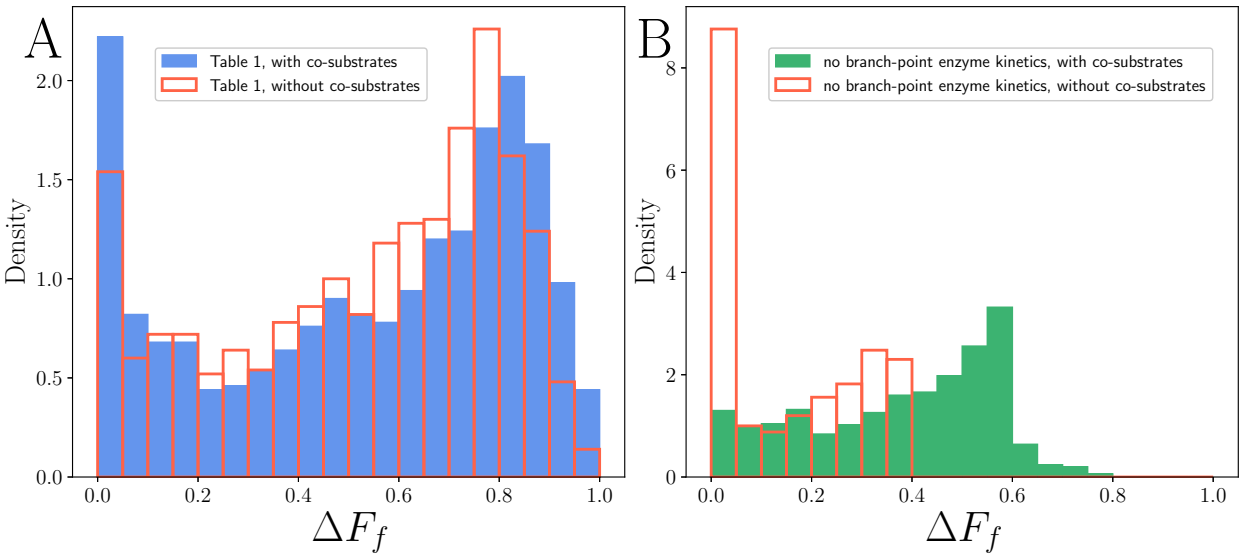

Figure S8: Co-substrate dynamics produce larger switches in the compartment model (A) Histograms for the distribution of ΔF_f in the case with/without co-substrates (blue/red). Parameters as in Table S1. (B) Histograms for the distribution of ΔF_f in the case with/without co-substrates (green/red) for the parameter regime shown in Table S1. but with all the reactions that have Pyruvate as a substrate set to have the same parameters to simulate the scenario without differential enzyme kinetics.

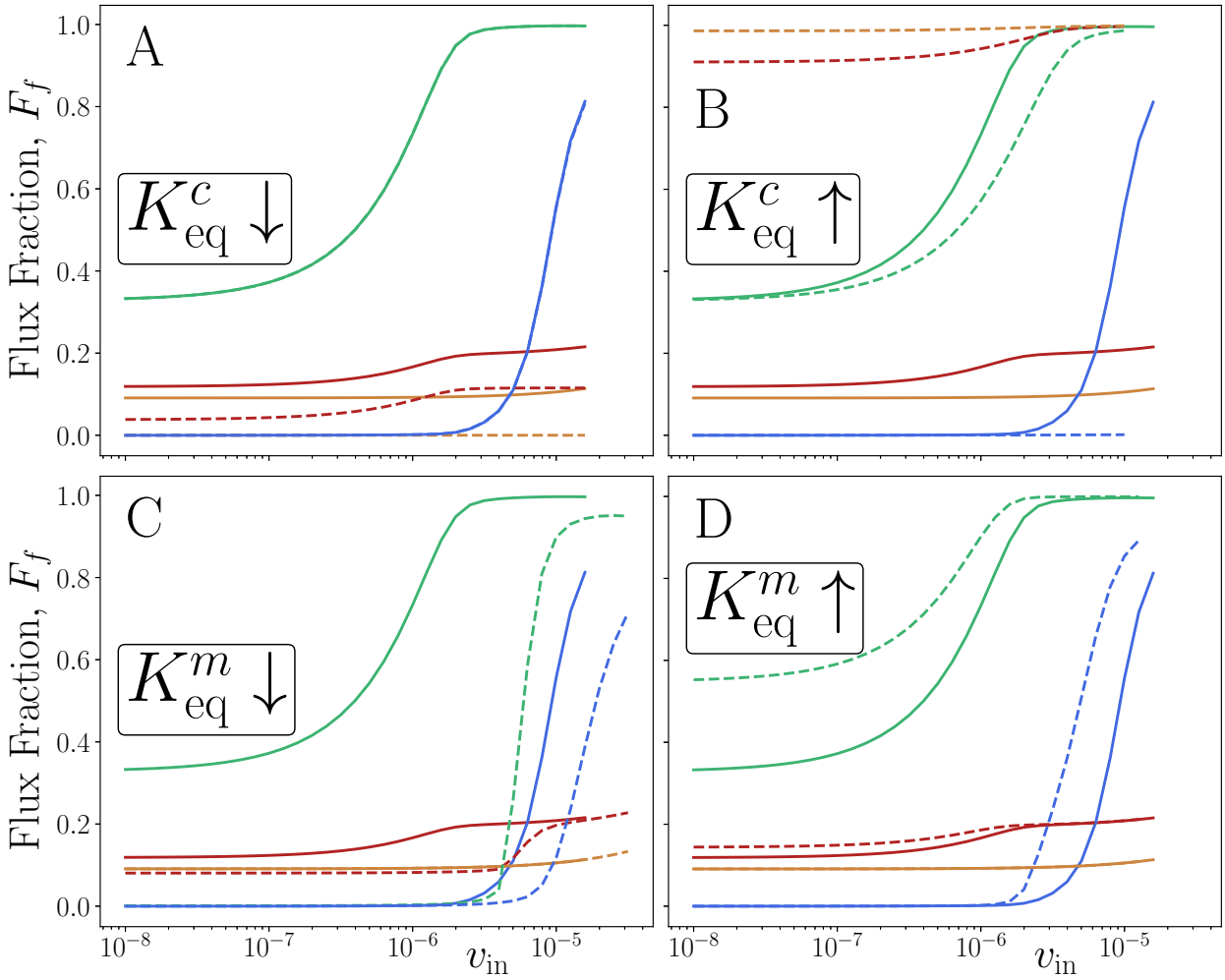

Figure S9: Mitochondrial co-substrates drive switching Effects of changing the NADH bias in the cytosol and mitochondria, by changing the K_{eq} for the background conversion (indicated in each panel). Solid lines are the same in all panels, and are the results from Fig. 4(E). Dashed lines show the effect of changing the cytosolic NADH levels (A,B) and the mitcohondrial NADH levels (C,D). Left column shows biasing towards NAD+, while the right column shows biasing towards NADH. Parameters are the same as in Fig. 4F, apart from the K_{eq} as indicated in each panel. Increased/Decreased K_{eq} means it is multiplied/divided by 10.

Michaelis-Menten (Reversible): $\nu = \frac{V_{\max}}{K}{}^{\mathrm{S}}_{\mathrm{M}} \frac{s - p/K_{\mathrm{eq}}}{1 + s/K^{\mathrm{S}}_{\mathrm{M}} + p/K^{\mathrm{P}}_{\mathrm{M}}}$						
Reaction (enzyme)	$V_{\max}$ (μmol/min/mg)	$K^{\mathrm{S}}_{\mathrm{M}}$ (mM)	$K^{\mathrm{P}}_{\mathrm{M}}$($mM$)	K_{eq}	Pool size (mM)	Citation(s)
GAP $\xleftrightarrow{\text{gapdh}}$ DPG	$1 - 10$	$0.001 - 1$	$0.001 - 1$	0.0056		[44]
DPG $\xleftrightarrow{\text{pgk1, gpm1, enolase}}$ PEP	$1 - 10$	$0.001 - 1$	$0.001 - 1$	$0.1 - 10$		[44]
PEP $\xleftrightarrow{\text{pyruvate-kinase}}$ PYR	$0.4 - 40$	0.014	0.53	$6.5 \cdot 10^3$		[44]
AcCHO $\xleftrightarrow{\text{adh}}$ EtOH	$0.3 - 30$	17	0.17	$1.45 \cdot 10^4$		[44]
AcCHO $\xleftrightarrow{\text{adh3}}$ EtOH	$0.3 - 30$	17	0.17	$1.45 \cdot 10^4$		[44]
NAD+ $\longleftrightarrow$ NADH	$0.06 - 6$	$0.01 - 10$	$0.01 - 10$	0.1	$0.3 - 3$	[16]*
NAD+ $\longleftrightarrow$ NADH	$0.04 - 4$	$0.1 - 100$	$0.001 - 1$	0.01	$0.03 - 0.3$	[16]*
Michaelis-Menten (Irreversible): $\nu = \frac{V_{\max}}{K_{\mathrm{M}}} \frac{m}{1 + m/K_{\mathrm{M}}}$						
Reaction (enzyme)	$V_{\max}$ (μmol/min/mg)	K_{M} (mM)	Citation(s)			
PYR $\xrightarrow{\text{pdc}}$ AcCHO	$0.03 - 3$	5	[44]			
PYR $\xrightarrow{\text{mcp}}$ PYR	$0.002 - 0.2$	$0.06 - 6$	[32]			
PYR $\xrightarrow{\text{pdh}}$ AcCoA	$0.01 - 1$	$0.06 - 6$	[8, 5]			
Inactive Transport (Linear): $\nu = v_{\mathrm{in}} s_{\mathrm{cyto}} - v_{\mathrm{out}} s_{\mathrm{mito}}$						
Reaction (enzyme)	v_{out} (min^{-1})	v_{in} (min^{-1})	Citation(s)			
AcCHO $\leftrightarrow$ AcCHO	$10^{-4} - 1$	$2 \cdot 10^{-4} - 1$				
EtOH $\leftrightarrow$ EtOH	$10^{-4} - 1$	$2 \cdot 10^{-4} - 1$				

Table S1: Parameters and parameter ranges used in the yeast model. All ranges are taken over a log-normal distribution. Colour indicates where the reaction happens: yellow, blue and yellow to blue for cytosol, mitochondria and cytosol into mitochondria respectively. Citations to studies used for obtaining parameters are given on the last column of the table. Note that the Pyr $\rightarrow$ Pyr reaction is an active transport reaction, which has the same functional form as an irreversible Michaelis-Menten reaction. In the case of simulations using 'fixed branch' parameters, the parameters for the mcp and pdh reactions are set to be equal to the parameters of the pdc reaction. * For cytosolic and mitochondrial NADH/NAD+, the citation was used for the pool size only.